Hierarchical porous MXene/amino carbon nanotubes-based molecular imprinting sensor for highly sensitive and selective sensing of fisetin.

MA, X., TU, X., GAO, F., XIE, Y., HUANG, X., FERNANDEZ, C., QU, F., LIU, G., LU, L. and YU, Y.

2020

Journal Pre-proof

Hierarchical porous MXene/amino carbon nanotubes-based molecular imprinting sensor for highly sensitive and selective sensing of fisetin

Xue Ma, Xiaolong Tu, Feng Gao, Yu Xie, Xigen Huang, Carlos Fernandez, Fengli Qu, Guangbin Liu, Limin Lu, Yongfang Yu

Hierarchical porous MXene/amino carbon nanotubes-based molecular imprinting sensor for highly sensitive and selective sensing of fisetin

Xue Ma[a,b], Xiaolong Tu[a], Feng Gao[a], Yu Xie[a], Xigen Huang[a], Carlos Fernandez[c], Fengli Qu[b,*], Guangbin Liu[a], Limin Lu[a*], Yongfang Yu[a]

[a]Key Laboratory of Crop Physiology, Ecology and Genetic Breeding, Ministry of Education, Key Laboratory of Chemical Utilization of Plant Resources of Nanchang, Institute of Functional Materials and Agricultural Applied Chemistry, College of Science, Jiangxi Agricultural University, Nanchang 330045, PR China

[b]College of Chemistry and Chemical Engineering, Qufu Normal University, Qufu Shandong 273165, P. R. China

[c]School of Pharmacy and Life Sciences, Robert Gordon University, Aberdeen, AB10-7GJ, UK

E-mail address: fengliquhn@hotmail.com (F, Qu), lulimin816@hotmail.com (L, Lu)

Tel.: +86 791 83813574; Fax: +86 791 83813574.

Graphical Abstract

A highly selective and sensitive electrochemical sensor based on hierarchical porous MXene/Amino carbon nanotubes (MXene/NH$_2$-CNTs) composite and molecularly imprinted polymer (MIP) was fabricated for detection of fisetin.
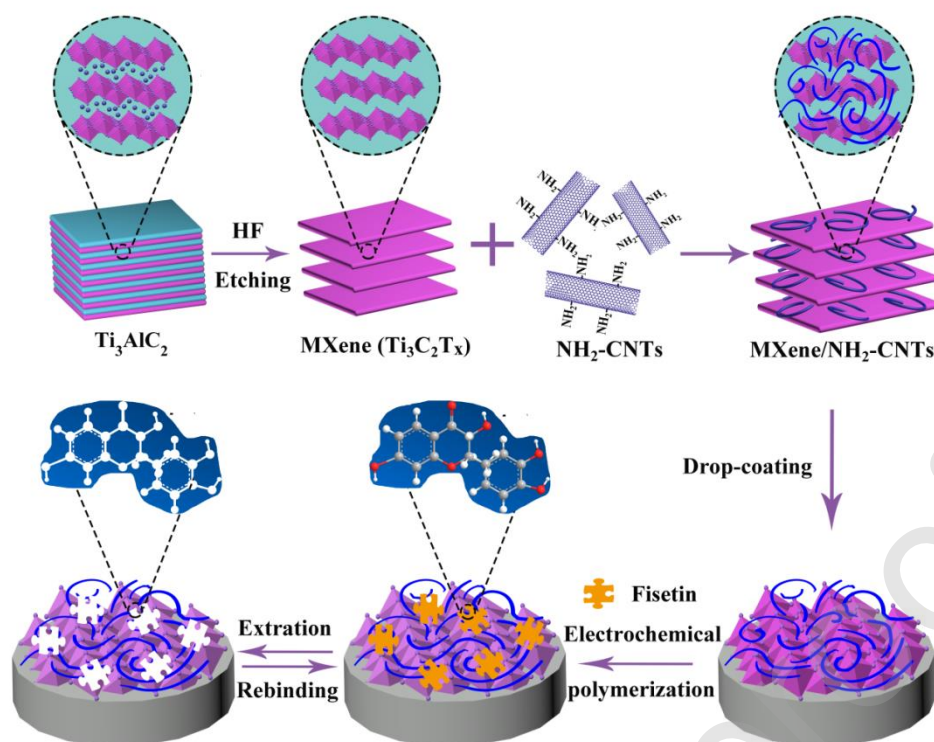
Highlights

- A novel molecularly imprinted sensor based MXene/NH2-CNTs composite was fabricated.

- NH2-CNTs as interlayer spacers efficiently prevented the aggregation of MXene.

- The combination of MXene/NH2-CNTs and MIP displays a favorable synergetic effect.

- This designed sensor achieved high sensitivity and selectivity detection of fisetin.

- The proposed method was applied in traditional Chinese medicine detection.

Abstract

In this work, a highly selective and sensitive electrochemical sensor based on hierarchical porous MXene/amino carbon nanotubes (MXene/NH$_2$-CNTs) composite and molecularly imprinted polymer (MIP) was developed for fisetin detection. The porous MXene/NH$_2$-CNTs films were fabricated by self-assembly of negatively charged Ti$_3$C$_2$T$_x$ MXene flakes and positively charged NH$_2$-CNTs. The utilization of conductive NH$_2$-CNTs as interlayer spacers efficiently inhibited the aggregation of MXene flakes and formed a well-defined porous structure, as a result of increasing the effective surface area, an enhancement of the electrical conductivity and electrocatalytic activity was observed. This sensor takes advantages of molecularly imprinted technique and MXene/NH$_2$-CNTs nanomaterials to achieve high selectivity and high sensitivity for the determination of fisetin. The factors that affect sensor response were studied and optimized. The as-prepared molecular imprinting sensor, under the optimized conditions, presented a good linear relationship with the fisetin concentration ranging from 0.003 μmol L^{-1} to 20.0 μmol L^{-1} with a limit of detection (LOD) of 1.0 nmol L^{-1}. Besides, with favorable stability and selectivity, this newly developed sensor was utilized for the detection of fisetin in actual samples with satisfactory results.

Keywords: Molecular imprinting sensor; Electrochemical detection; MXene; NH$_2$-CNTs; Fisetin

1. Introduction

Fisetin is a flavonoid species widely distributed in plants with physiological activities like anti-oxidation, anti-aging, anti-inflammatory and antibacterial effects [1, 2]. Fisetin has caused widespread concern owing to its strong antioxidant characteristics and has been widely used in clinical chemistry and human health [3]. In view of these, the precise and sensitive detection of fisetin is of great importance. Currently, high performance liquid chromatography (HPLC) has been widely used in the detection of fisetin [4]. This method is efficient and reliable, but the operating instrument is expensive and the program is complicated. By contrast, electro-analytical techniques have the advantages of fast response, low cost, easy operation and short operation time [5-8]. Moreover, it has been verified that electrode material and structure play an important role to realize high detection sensitivity. As far as we know, there are few reports on the electrochemical detection of fisetin. For example, Daniela et al. have reported the gold nanoparticles and silica in ionic liquids composite as an electrode material for determination of fisetin with LOD of 0.28 μmol L^{-1}[3]. Maza et al. have prepared thiol self-assembled monolayer modified gold electrode for electrochemical determination of fisetin and obtained a LOD to be 0.5 μmol L^{-1} [9]. However, the sensitivity of these sensors still needs to be improved. Therefore, it is imperative to exploit new electrochemical sensing substrates.

MXene is a newly emerging transition metal carbide and nitride material with the

general formula $M_{n+1}X_nT_x$, where M represents early transition metals, X denotes C or N, T_x represents surface functional groups (-O, -OH, -F), and n is 1-3. Because of its advanced energy storage performance, good metallic conductivity and excellent mechanical properties, MXene has great application prospects in supercapacitor applications [10, 11], catalysts [12, 13] and lithium-sulfur batteries [14, 15]. Especially, as MXene has a huge specific active area and good conductivity, it has attracted a lot of attention as a promising electrode material for electrochemical sensors. For example, MXene-Ti_3C_2 based sensor electrode has been utilized for the detection of chemical and biomolecules, such as nitrite [16], dopamine [17], carcinoembryonic antigen [18], etc. Although MXene exhibits these advantages, the intrinsic 2-D structures of MXene put up with re-stacking, which limits their electrochemical properties and hinders target molecules accessed to the active material [19, 20].

Recent research demonstrated that the introduction of interlayer spacers, such as one-dimensional carbon nanotubes (CNTs), between the sheets is an effective way to avoid the aggregation of MXene [21-23]. For instance, Zhang et al. prepared $Ti_3C_2T_x$/CNTs flexible self-supporting composite film through vacuum filtration method for high-performance lithium-ion capacitors [22]. Gogotsi et al. fabricated sandwich-like MXene/CNTs composite paper electrodes through alternating filtration of MXene and CNTs dispersions for high volumetric capacitance [24]. Shao et al. designed sandwich-like $Ti_3C_2T_x$ MXene/CNTs strain sensing layers by using delaminated $Ti_3C_2T_x$ flakes and hydrophilic CNTs via layer-by-layer (LBL) spray

5

coating technique [25]. Nevertheless, the random physical mixing of MXene with CNTs cannot efficiently prevent the self-restacking of MXene because both CNTs and MXene carry negative charge on their surface. Besides, there is weak bonding between them. In this aspect, Wang et al. [19] reported the fabrication of porous Ti_3C_2 MXene/CNTs composite through electrostatic self-assembly between positively charged CNTs modified with cationic surfactant cetyltrimethylammonium bromide (CTAB) and negatively charged $Ti_3C_2T_x$ MXene. The negatively charged CTAB-CNTs can effective inhibit the reunion of MXene. However, the non-conductive surfactant increased the electron transfer resistance, which decreased the electrical properties of the composite. By comparison, amino functionalized CNTs (NH_2-CNTs) not only own good conductivity, but also have negative electricity on their surface, and yet there is no report on MXene/NH_2-CNTs hybrid as the electrode material for an electrochemical sensor. The MXene/NH_2-CNTs hybrid combines the properties of MXene with NH_2-CNTs and is expected to present excellent electrochemical sensing performance.

In addition, selectivity is another bottleneck that plagues the application of sensors in tracking measurements. Molecularly imprinted polymers (MIP) can be viewed as a modified material that enhances selectivity of sensors with specific recognition property, low cost and short synthesis time. In the MIP synthesis process, a molecular recognition site with specificity in shape and size to the template molecules is generated [26]. Compared to non-conductive polymers, conducting polymers were considered as one of the best candidates for the synthesis of MIPs for

6

selective recognition [27]. Among the conducting polymers, polypyrrole (ppy) is widely used in molecular imprinting sensors because of its advantages such as high electrical conductivity, convenient synthesis, environment-friendly and good catalytic performance [28-30]. For instance, Tan et al. have synthesized grapheme quantum dot composites for detection of bisphenol A with MIP using ppy as polymer material, demonstrating high selectivity of MIP sensor, which exhibited a fine linear relationship range from 0.1 $\mu mol\ L^{-1}$ to 50.0 $\mu mol\ L^{-1}$ with LOD of 0.04 $\mu mol\ L^{-1}$ [31]. Qian et al. have developed molecular imprinting technology based on ppy imprinted polymer coated CNTs and a low LOD of 1.0×10^{-11} mol L^{-1} was obtained [30]. The introduction of ppy not only showed good catalytic performance, but also enhanced the selectivity of molecular imprinting sensing. Considering the merits of CNTs/Ti_3C_2 hybrids and the selectivity from MIP, it is of great significance to explore MXene/NH_2-CNTs based ppy MIP sensor for fisetin detection.

Herein, we demonstrated the preparation of MXene/NH_2-CNTs by self-assembly of negatively charged $Ti_3C_2T_x$ flakes and positively charged NH_2-CNTs, which was thus coupled with MIP for the fabrication of a novel electrochemical sensor for fisetin detection. The prepared MIP layer provides ultra-specificity for fisetin sensor. MXene and NH_2-CNTs have synergistic fast electron transfer capability, large electrochemical area and favorable catalytic activity, which can help to amplify the electrochemical signal and thus enhance the sensitivity of the sensor. By using the DPV, the electrochemical sensor exhibited a wide linear concentration range from 0.003 μmol L^{-1} to 20.0 $\mu mol\ L^{-1}$ with a low LOD of 1.0 nmol L^{-1}. Furthermore, the

MIP/MXene/NH$_2$-CNTs sensor demonstrated an excellent stability and reproducibility, and was successfully utilized for the detection of fisetin in cotinus coggygria leaves sample.

2. Experimental section

2.1 Materials and reagents

Amino carbon nanotube (NH$_2$-CNTs) and Ti$_3$AlC$_2$ powder were purchased from Nanjing XF Nano Co, Ltd. Hydrochloric acid (HCl) and lithium fluoride (LiF), cetyl trimethyl ammonium bromide (CTAB), K$_3$[Fe(CN)$_6$], K$_4$Fe(CN)$_6$, and KCl were supported by Vita Reagent Co., Ltd. Phosphate buffers (PBS, 0.1 mol L^{-1}) were obtained using Na$_2$HPO$_4$ and Na$_2$HPO$_4$. The different pH of PBS solution was adjusted by phosphoric acid (H$_3$PO$_4$, 0.1 mol L^{-1}) and sodium hydroxide (NaOH, 0.1 mol L^{-1}). All reagents were analytical grade pure and did not require any purification or pretreatment.

2.2 Apparatus

Electrochemical detection was conducted on the CHI760D electrochemical workstation (Shanghai, China). A conventional three-electrode system consisting of saturated calomel electrode, platinum wire electrode and glass carbon electrode (GCE, Φ= 3 mm) were used for all electrochemical experiments. The morphologies of composites were recorded by scanning electron microscopy (SEM) (Hitachi S4800, Japan). X-ray photoelectron spectroscopy (XPS) was operated on a Thermo VG Scientific ESCA Lab 250 instrument using Al Kα radiation. X-ray powder diffraction

(XRD) spectra were performed on Lab XRD-6000 X-ray diffractometer using Cu Kα

radiation.

2.3 Synthesis of multilayered MXene (Ti$_3$C$_2$T$_x$) and MXene/NH$_2$-CNTs composite

The multilayered MXene (Ti$_3$C$_2$T$_x$) was synthetized according to the literature

with a little modification [20]. Typically, LiF powder (1 g) was dissolved in 20 mL

HCl solution (9 mol L^{-1}). The Ti$_3$AlC$_2$ material was slowly added into the above

solution and the mixture was stirred for 24 h at 40 °C. The resulting products were

washed with deionized (DI) water for three times and centrifuged at 3500 rpm for 10

min, and washed with deionized water until the liquid supernatant pH was above 6.

The obtained MXene (Ti$_3$C$_2$T$_x$) powder was dried at 60 °C for 24 h.

The preparation process of the MXene/NH$_2$-CNTs composite was as follows:

NH$_2$-CNTs dispersion (0.5 mg mL^{-1}) was obtained by dissolving 2 mg NH$_2$-CNTs

into 4 mL 0.1 wt% CTAB solution. Then, the prepared NH$_2$-CNTs (3.1 mL) solution

was added to Ti$_3$C$_2$T$_x$ suspension (0.4 mg mL^{-1}, 35 mL) drop by drop. The mixture

was sonicated for 1 h and the MXene/NH$_2$-CNTs composite was washed repeatedly

with water and dried in a vacuum oven for 8 h.

2.4 Preparation of MIP/MXene/NH$_2$-CNTs modified electrode

Before modifying the electrode, GCE was polished on the chamois leather for 10

min until a bright mirror appeared and rinsed repeatedly with DI water and ethanol.

5 μL MXene/NH$_2$-CNTs dispersion (1 mg mL^{-1}) was dripped onto the surface of

the pre-prepared GCE and dried under infrared lamp to obtain MXene/NH$_2$-CNTs

/GCE.

The MXene/NH$_2$-CNTs/GCE was then immersed in 0.1 mol L^{-1} PBS containing 0.1 mol L^{-1} lithium perchlorate (LiClO$_4$) solution, 2 mmol L^{-1} pyrrole (py) and 0.4 mmol L^{-1} fisetin. Cyclic voltammetry (CV) was employed to carry out the electro-polymerization process in the potential range from -0.6 V to 1.8 V with the scan rate of 50 mV s^{-1} for 8 cycles. After that, the obtained electrode was immersed in a mixed solution containing 0.2 mol L^{-1} sodium hydroxide (NaOH) and ethanol (V/V: 1:1) for 20 min to elute the fisetin template under micro-stirring conditions. NaOH provides a good alkaline environment, which is able to destroy the electrostatic force between fisetin and pyrrole, enabling fisetin to be eluted. Thus, the MIP/MXene/NH$_2$-CNTs/GCE was obtained. The preparation process of MIP/MXene/NH$_2$-CNTs/GCE is illustrated in Scheme 1.

The non-imprinted polymer modified electrode (NIP/MXene/NH$_2$-CNTs/GCE) was also synthesized by the same method, but without the addition of fisetin in the electro-polymerization process.

2.5. Electrochemical measurements

The MIP/MXene/NH$_2$-CNTs/GCE was immersed in 0.1 mol L^{-1} PBS solution containing different concentration of fisetin under mild magnetic stirring for 150 s to re-incubate the fisetin. Cyclic voltammetry (CV) or differential pulse voltammetry (DPV) was operated at the potential of -0.2 V - 0.6 V at a scan rate of 100 mV s^{-1}.

2.6 Preparation and analysis of samples

To investigate the application of the actual sample, cotinus coggygria leaves were obtained from the local store. The cotinus coggygria leaves sample was dried at

80 °C and then pulverized. The sample was dispersed into 10 mL ethanol with

vigorously stirring. Next, the sample solution was centrifuged on a centrifuge of 5000

rpm for 10 min to remove insoluble impurities. 1 mL sample solution was diluted to

30 mL with 0.1 mol L^{-1} PBS (pH 7.0). The supernatant was reserved in a 4 °C

refrigerator for subsequent experiments.

3. Results and Discussion

3.1 Characterization of MXene/NH$_2$-CNTs

The morphologies of composites were obtained by SEM. As shown in Fig. 1A, a

typical MXene multi-layered structure similar to an accordion was observed. From the

Fig. 1B, dense NH$_2$-CNTs were uniformly distributed in the interlayers of MXene

sheets. MXene was bridged by curved NH$_2$-CNTs, gradually crossing linked into a

nano-porous network, facilitating electron transfer and proton transport. Moreover,

the connected NH$_2$-CNTs as interlayer spacers were intercalated in MXene flakes,

which effectively avoid the re-stacking of MXene.

After the electro-polymerization on MXene/NH$_2$-CNTs/GCE, a smooth and

uniform ppy film was observed (Fig. 1C). Subsequently, the extraction of fistin

molecules lead to more pores on the MXene/NH$_2$-CNTs surface (Fig. 1D), and the

increased surface porosity suggested that template molecules were successfully eluted

from the polymer. Compared with the MIP/MXene/NH$_2$-CNTs/GCE, the surface of

NIP/MXene/NH$_2$-CNTs/GCE (Fig. 1E) became much hazy and dense. For the

MIP/GCE (Fig. 1F), rough surfaces were observed, indicating the MIP/GCE has a

specific imprinted sites. These results suggested the molecularly imprinted caves were

11

successfully coated on the surface of MXene/NH$_2$-CNTs nanocomposite.

X-ray Photoelectron Spectroscopy (XPS) was employed to research the elemental valence and surface functional groups of MXene and MXene/NH$_2$-CNTs composite. Fig. 2A demonstrates the survey XPS spectrum of MXene (a) and MXene/NH$_2$-CNTs (b), which mainly contains five elements corresponding to C, N, Ti, O, F element. For MXene/NH$_2$-CNTs (b), the intensity of C 1s was increased obviously in relation with MXene (a), indicating the presence of abundant NH$_2$-CNTs on the surface of Ti$_3$C$_2$T$_x$ [32]. The high-resolution XPS spectra of C 1s (Fig. 2B) could be decomposed into five components. The peaks at 284.3 284.5, 284.9, 285.3 and 285.9 eV might be assigned as C-Ti, C-C, C-N, C-O and O-C=O, respectively [33]. The Ti 2p spectra of MXene/NH$_2$-CNTs (Fig. 2C) were also studied. Four functional groups appeared at 455.2, 456.6, 461.3 and 467.5 eV, which were associated with Ti-C, Ti (ii), Ti-F and Ti-O, respectively [34]. The XPS spectra of O 1s are presented in Fig. 2D. The peaks at 531.5, 532.3 and 533.6 eV were ascribed to the C-O, O=C-N and C=O group, whereas the peak at 533.2 eV was assigned with the Ti-O bond [35].

The phase and crystal structure of pure MXene and MXene/NH$_2$-CNTs were characterized by X-ray diffraction spectroscopy (XRD). As illustrated in Fig. 3a, the diffraction pattern of the MXene demonstrated intense (002), (004) and (006) peaks, indicating that the prepared material had 2D layered structure [36]. The major diffraction characteristic peaks of MXene were observed at 8.9°, 16.2°, 27.6°, 34.5°, 36.4°, 43.2° and 60.6°, corresponding to the (002) (004) (006), (100) (101), (103) and (110) lattice plane of Ti$_3$C$_2$T$_x$ [37]. For the MXene/NH$_2$-CNTs composite (Fig. 3b),

characteristic diffraction peaks of MXene were detected as the main crystalline phase. In addition, typical peaks of NH$_2$-CNTs appeared at 26.3°, which corresponded to the (002) of NH$_2$-CNTs (JCPDS No. 75-1621) [32]. These results indicated that the successful synthesis of the MXene/NH$_2$-CNTs.

3.2 Electrochemical behavior of modified electrodes

Electrochemical impedance spectrum (EIS) was used for evaluating modified electrode's charge-transfer ability. The diameter of the semicircular plot in the EIS spectrum represents the charge transfer resistance (Rct). As shown in Fig. 4A, the typical Nyquist plots of (a) bare GCE, (b) MXene/GCE, (c) NH$_2$-CNTs/GCE and (d) MXene/NH$_2$-CNTs/GCE were recorded in 5 mmol L^{-1} [Fe(CN)$_6$]$^{3-/4-}$ solution containing 0.1 mol L^{-1} KCl. The equivalent circuit (inset of Fig. 4A) was performed to simulate the Nyquist plots, which consists of a charge transfer resistance (Rct), and a Warburgh impedance (W), a constant phase element (CPE, it is a double-layer capacitance Cdl in this work) and an active electrolyte resistance (Rs).

By fitting the impedance data from the Nyquist plots on the basis of the Randle's equivalent circuit model, the Rct values of bare GCE, MXene/GCE and NH$_2$-CNTs/GCE were estimated to be 439.12 Ω, 28.87 Ω and 25.05 Ω, respectively. These data imply MXene and NH$_2$-CNTs own the excellent electrical conductivity. Moreover, it was found that the Rct value of MXene/NH$_2$-CNTs/GCE decreased to 18.45 Ω, which was much lower than those of MXene/GCE and NH$_2$-CNTs/GCE, suggesting the successful synthesis of the MXene/NH$_2$-CNTs.

The construction of the modified electrodes was studied by CV range from -0.2

V to 0.6 V at a scan rate of 100 mV s^{-1} with $[Fe(CN)_6]^{3-/4-}$ as the redox probe. As presented in Fig. 4B, a pair of well-defined redox characteristic peaks appeared at bare GCE (curve a). After GCE was modified with MXene/NH$_2$-CNTs, the redox peak currents increased remarkably (curve b), indicating that MXene/NH$_2$-CNTs showed an excellent electronic conductivity and huge active area which aided to accelerate the electron transfer. However, the peak current decreased (curve c) before the removal of the template. This was because the MIP film before removing the template was almost non-conductive, blocking the probe from entering the electrode surface. After the template molecules were removed, the peak current enhanced significantly (curve d), due to the formation of some channels or binding cavities which caused the probe to arrive into the surface of the GCE through the MIP film. Nevertheless, the peak currents decreased apparently (curve e) after incubating into 0.1 mol L^{-1} PBS (pH 7.0) containing 20.0 μmol L^{-1} fisetin solution for 150 s. This could be ascribed to the binding cavities of the MIP film recombined with fisetin, thus hindered the redox probe arrival onto the electrode surface.

To prove the merits of the MIP sensor, CV curves of fisetin at bare GCE (a), MIP/GCE (b), NIP/MXene/NH$_2$-CNTs/GCE (c) and MIP/MXene/NH$_2$-CNTs/GCE (d) in 0.1 mol L^{-1} PBS (pH 7.0) after incubation in 20.0 μmol L^{-1} fisetin for 150 s were investigated (Fig. 4C). As shown, a pair of weak redox peaks corresponding to the electrochemical oxidation and reduction of fisetin appeared at bare GCE (a) and MIP/GCE (b). However, for NIP/MXene/NH$_2$-CNTs/GCE (c) and MIP/MXene /NH$_2$-CNTs/GCE (d), larger redox peaks were observed, indicating that

14

MXene/NH$_2$-CNTs could enhance the electrocatalytic activity and improve the sensing performance toward fisetin. In addition, MIP/MXene/NH$_2$-CNTs/GCE (d) showed higher redox currents than that at NIP/MXene/NH$_2$-CNTs/GCE (c), indicating that the formation of imprinted cavities can produce highly selective recognition sites and enhanced the catalytic oxidation of fisetin. Moreover, compared with MIP/GCE (b), a pair of redox peaks with higher currents were observed in MIP/MXene /NH$_2$-CNTs/GCE (d), suggesting the excellent catalytic oxidation of MXene/NH$_2$-CNTs that promoted electron transfer and proton transport. These results proved the superiority of MIP/MXene/NH$_2$-CNTs for fisetin detection.

3.3 Optimization of conditions

To enhance the sensitivity and selectivity of the MIP sensor, some factors including the polymerization cycles, the ratio of functional monomer to template molecule, extraction time, pH of supporting electrolyte and incubation time were evaluated. DPV technique was employed to investigate electrochemical performance in 0.1 mol L^{-1} PBS containing 20.0 μmol L^{-1} fisetin.

As it is known, the thickness of MIP film often affects the amount of imprinted fisetin cavities, which can be adjusted by controlling the number of cycles for electropolymerization. Fig. 5A showed the influence of polymerization cycles on the current response. The oxidation peak current of fisetin increased proportionally with the polymerization cycles, indicating the formation of more imprinting sites. The maximum peak current was obtained at 8 cycles. However, when polymerization cycles exceed 8, the oxidation peak current decreased, indicating that the polymer

15

film was too thick to completely remove the template molecule [38]. Therefore, the optimal polymerization cycles was chosen to be 8 cycles.

The ratio of monomer/template has an impact on the amount of the imprinted sites in the polymer matrix, which further affects the property of the MIP sensor. Fig. 5B displayed the effect of different ratios of monomer and template (2:1 to 8:1) on the current response. As shown, with the increase of monomer, the peak current increased continuously. The possible reason was that less monomers cannot bind enough template molecules, resulting in fewer number of recognition sites in the MIP film [39]. The maximum current value of the oxidation peak can be observed when the ratio of monomer to template was 5: 1. However, further increasing the ratio of monomers, the current decreased. This was because an excess of monomer led to a reduced recognition site or binding cavity [40]. As a result, the ratio of the monomer to the template was selected as 5:1.

The influence of extraction time on template molecules was investigated (Fig. 5C). With the prolongation of the extraction time, the current response increased continuously, indicating that the template molecules were gradually removed. When the extraction time increases from 20 min to 35 min, the current was decreased, suggesting that excessive extraction time may destroy the surface of the polymer film [39]. Thus, 20 min was selected as the best extraction time.

The influence of pH value on the current response of fisetin was optimized in the range from 4.0 to 9.0. From Fig. 5D, with the increase the pH value of the detection solution, the peak potential moved to the negative direction, showing that protons

16

participated in electrochemical reactions. Moreover, the oxidation peak potential was linear with the pH and the corresponding equation was found to be: $E_{pa}/V = 0.778 - 0.062$ pH ($R^2 = 0.998$). The slope of the equation is close to the theoretical value of 59 mV pH^{-1}, which proved that equal number protons and electrons participated in electrochemical reaction [41].

In addition, the maximum oxidation peak current was obtained at pH 6.0, which might be due to the potential destruction of MIP film in overly acidic or alkaline PBS solutions [42]. Hence, pH 7.0 was identified as the optimal support electrolyte solution.

To investigate the adsorption degree of the analyte on the electrode surface, the influence of incubation time on the peak current for MIP sensor was studied. Fig. 5E exhibits that the peak current increased by increasing the incubation time. When the incubation time reached 150 s, the peak current remained almost unchanged, implying that the adsorption of fisetin on the electrode surface reached saturation [43]. So, 150 s was chosen as the most appropriate incubation time.

3.4 Kinetic study of fisetin at MIP/MXene/NH$_2$-CNTs/GCE

The kinetic reaction mechanism of the MIP/MXene/NH$_2$-CNTs/GCE was investigated by CV at different scanning rates in 0.1 mol L^{-1} PBS solution (pH 7.0) containing 20.0 μmol L^{-1} fisetin. As depicted in Fig. 6A, the redox peak current increased when the scan rate increased from 20 to 300 mV s^{-1}. Besides, a good linear relationship was obtained between the oxidation reduction peak current and the scan rate (Fig. 6B). The linear equation were $I_{pa} = 5.817 + 0.104\ v$ ($R^2 = 0.995$) and $I_{pc} =$

-2.266 - 0.098 v (R^2= 0.993), respectively, indicating that the reaction mechanism of kinetics was controlled by a diffusion process [44].

Additionally, the redox peak potential (E_p) and the natural logarithm of scan rate (ln v) showed a good linear relationship (Fig. 6C). Linear equations can be expressed as E_{pa}= 0.167 + 0.052 ln$v$ (R^2= 0.996) and E_{pc}= -0.219 - 0.043 ln$v$ (R^2= 0.995), respectively. According to the Ravilon equation [45], the slope of the equation for E_{pa} and E_{pc} could be represented as 2.3RT/n(1-α)F and 2.3RT/nαF, respectively. Thus, the electron transfer number (n) and the electron transfer coefficient (α) were calculated as 2 and 0.55, respectively. Combined with the results of the pH, the electrochemical reaction of fisetin involved the participation of two electrons and two protons (Scheme 2).

3.5 Sensor performance

To evaluate the analytical performance of the MIP sensor, DPV technique was employed to investigate the different concentrations of fisetin under optimized conditions. As depicted in Fig. 7, with the increase of fisetin concentration, the oxidation peak current increased. It was found that the oxidation peak current was linear to the fisetin concentration in the range from 0.003 μmol L^{-1} to 20.0 μmol L^{-1} with the linear equation of I (μA) = 0.981 + 0.964 c (μmol L^{-1}) (R^2= 0.995). The limit of detection (LOD) is 1.0 nmol L^{-1}, which was calculated using the following equations [46-47]:

$$LOD = 3 \times SD/S$$

Where, SD is the standard deviation for ten replicates determination of the blank

signal and S is the slope of the calibration curve).

The analytical performance comparison between the reported electrode sensors and our method was summarized in Table 1. As shown, the sensor constructed in this work shows a lower LOD. The excellent performance obtained at the MIP/MXene/NH$_2$-CNTs/GCE mainly resulted from the synergistic effects of the MXene/NH$_2$-CNTs composite and the specific recognition of the MIP. Firstly, NH$_2$-CNTs inserted in MXene prevented aggregation, thus further increased the effective surface area and provided abundant active sites. Secondly, MXene/NH$_2$-CNTs with a layered structure and a good conductivity offered an open channel for electron transport, which facilitated electron transfer. Thirdly, the specific recognition sites of MIP film exhibit highly affinity for the template molecule-fisetin, which enhanced the sensitivity and selectivity.

3.6 Selectivity, reproducibility and stability

Selectivity is an important indicator for evaluating molecular imprinting sensor. The potential interferences of substances such as caffeic acid, citric acid, chlorogenic acid, rutin, oxalic acid, and quercetin were investigated using DPV in the presence of 20.0 μmol L^{-1} fisetin. As shown in Fig. 8A, the results revealed that there was no obvious influence after 50-folds interference substances were added. The peak current change was below 5%. The results verified the excellent selectivity and specificity of the MIP sensor, which can be ascribed to the fact that the abundant cavities within the polymer matrix were complementary in size, shape and functionality to the template-fisetin.

19

The reproducibility was evaluated by using six independent MIP-MXene/ NH$_2$-CNTs/GCEs under the same conditions, which were used to determine 20.0 μmol L^{-1} fisetin, respectively. Fig. 8B suggested that the RSD of the peak currents was 3.43%, showing the sensor owns satisfactory reproducibility. In addition, the long-term stability of MIP-MXene/NH$_2$-CNTs/GCE was assessed by monitoring 20.0 μmol L^{-1} fisetin intermittently after storage at room temperature for five weeks. The modified electrode was tested every two days. The results (Fig. 8C) showed that the change of the measured current value was only 3.06% of the original current value after five weeks of storage, indicating good stability of the MIP sensor.

3.7 Application of MIP-MXene/NH$_2$-CNTs/GCE for real sample analysis

To evaluate the feasibility of the developed MIP sensor, the MIP-MXene/ NH$_2$-CNTs/GCE was used to determine fisetin in cotinus coggygria leaves sample. The samples were pretreated as depicted in Section 2.6. After that, the content of fisetin in practical sample was researched by a standard addition method. Obviously, there is no oxidation peak when no fisetin was added in the pre-sample solution. When different fisetin (1.00 μmol L^{-1}, 3.00 μmol L^{-1}, 5.00 μmol L^{-1}, 10.00 μmol L^{-1} and 20.00 μmol L^{-1}) concentrations were added, apparent oxidation peaks at 0.208 V were observed. Relevant results were listed in Table 2. As shown, satisfactory recoveries were obtained between 98.7% and 103.0% and the RSD was less than 5%.

For comparison, the concentrations of fisetin in the above samples were detected by high performance liquid chromatography (HPLC). As shown in Fig. 9, the obtained results from HPLC and the MIP-MXene/NH$_2$-CNTs/GCE were in good agreement.

These results showed that the designed method can be successfully used for practical samples. These results showed that the designed method can be successfully used for practical samples.

4. Conclusion

In summary, a highly sensitive and selective molecular imprinting sensor was fabricated based on MXene/NH_2-CNTs substrate material. The MIP layer cavity network of the fisetin molecule can simultaneously identify and quantify fisetin, ensuring its high selectivity. The hierarchical porous MXene/NH_2-CNTs composite effectively provided large electrochemical area and excellent conductivity. The combination of MXene/NH_2-CNTs and MIP displayed a favorable synergetic effect for the electro-catalytic oxidation of fisetin. Based on these advantages, the obtained MIP/MXene/NH_2-CNTs/GCE showed a high analytical performance for fisetin determination with a LOD of 1.0 nmol L^{-1}. In addition, the modified electrode was successfully applied to detect fisetin in cotinus coggygria leaves with good recoveries. The method described here provides a new molecular imprinting technique for simple, low cost, selective and sensitive determination of flavonoid. Therefore, it can be expected that the developed sensor could be readily extended for detection of other traditional Chinese Medicine.

Declaration of Interest Statement

There are no any competing financial interests or personal relationships that could have appeared to influence the work reported in this paper.

Acknowledgements

Reference

[1] A. Şenocak, B. Köksoy, E. Demirbaş, T. Basova, M. Durmuş, 3D swcnts-coumarin hybrid material for ultra-sensitive determination of quercetin antioxidant capacity, Sens. Actuators B 267 (2018) 165-173.

[2] G. Li, L. Liu, Y. Cheng, S. Gong, X. Wang, X. Geng, W. Sun, Electrochemical behavior of luteolin on a chitosan-graphene modified glassy carbon electrode and its sensitive detection, Anal. Methods 6 (2014) 9354-9360.

[3] D. Brondani, I. C. Vieira, C. Piovezan, J. M. Ramos da Silva, A. Neves, J. Dupont, C. W. Scheeren, Sensor for fisetin based on gold nanoparticles in ionic liquid and binuclear nickel complex immobilized in silica, Analyst 135 (2010) 1015-1022.

[4] F. Fang, J. M. Li, Q. H. Pan, W. D. Huang, Determination of red wine flavonoids by HPLC and effect of aging, Food. Chem. 101 (2007) 428-433.

[5] W. Cao, Y. Wang, Q. Zhuang, L. Wang, Y. Ni, Developing an electrochemical sensor for the detection of tert-butylhydroquinone. Sens. Actuators B, 293 (2019) 321-328.

[6] V. M. Ekomo, C. Branger, R. Bikanga, A. M. Florea, G. Istamboulie, C. Calas-Blanchard, T. Noguer, A. Sarbu, H. Brisset, Detection of Bisphenol A in aqueous medium by screen printed carbon electrodes incorporating electrochemical molecularly imprinted polymers, Biosen. Bioelectron. 112 (2018) 156-161.

[7] H. Rao, X. Zhao, X. Liu, J. Zhong, Z. Zhang, P. Zou, Y. Jiang, X. Wang, Y. Wang, A novel molecularly imprinted electrochemical sensor based on graphene quantum

dots coated on hollow nickel nanospheres with high sensitivity and selectivity for the rapid determination of bisphenol S, Biosens. Bioelectron. 100 (2018) 341-347.

[8] Y. Wang, W. Cao, L. Wang, Q. Zhuang, Y. Ni, Electrochemical determination of 2, 4, 6-trinitrophenol using a hybrid film composed of a copper-based metal organic framework and electroreduced graphene oxide. Microchim. Acta, 185 (2018) 315-324.

[9] E. Maza, H. Fernández, M. A. Zon, M. B. Moressi, Electrochemical determination of fisetin using gold electrodes modified with thiol self-assembled monolayers, J. Electroanal. Chem. 790 (2017) 1-10.

[10] L. Yu, L. Hu, B. Anasori, Y. T. Liu, Q. Zhu, P. Zhang, Y. Gogotsi, B. Xu, MXene-bonded activated carbon as a flexible electrode for high-performance supercapacitors, ACS Energy Lett. 3 (2018) 1597-1603.

[11] C. Yu, Y. Gong, R. Chen, M. Zhang, J. Zhou, J. An, F. Lv, S. Guo, G. Sun, A solid-state fibriform supercapacitor boosted by host-guest hybridization between the carbon nanotube scaffold and MXene nanosheets, Small 14 (2018) 1203-1210.

[12] O. Mashtalir, K. M. Cook, V. N. Mochalin, M. Crowe, M. W. Barsoum, Y. Gogotsi, Dye adsorption and decomposition on two-dimensional titanium carbide in aqueous media, J. Mater. Chem. A. 2 (2014) 14334-14338.

[13] Z. W. Seh, K. D. Fredrickson, B. Anasori, J. Kibsgaard, A. L. Strickler, M. R. Lukatskaya, Y. Gogotsi, T. F. Jaramillo, A. Vojvodic, Two-dimensional molybdenum carbide (MXene) as an efficient electrocatalyst for hydrogen evolution, ACS Energy Lett. 1 (2016) 589-594.

[14] X. Liang, Y. Rangom, C. Y. Kwok, Q. Pang, L. F. Nazar, Interwoven MXene nanosheet/carbon-nanotube composites as Li-S cathode hosts, Adv. Mater. 29 (2017) 40-47.

[15] X. Liang, A. Garsuch, L. F. Nazar, Sulfur cathodes based on conductive MXene nanosheets for high-performance lithium-sulfur batteries, Angew. Chem. 54 (2015) 3907-3911.

[16] H. Liu, C. Duan, C. Yang, W. Shen, F. Wang, Z. Zhu, A novel nitrite biosensor based on the direct electrochemistry of hemoglobin immobilized on MXene-Ti_3C_2, Sens. Actuators B 218 (2015) 60-66.

[17] F. Shahzad, A. Iqbal, S. A. Zaidi, S. W. Hwang, C. M. Koo, Nafion-stabilized two-dimensional transition metal carbide ($Ti_3C_2T_x$ MXene) as a high-performance electrochemical sensor for neurotransmitter, J. Ind. Eng. Chem. 25 (2019) 338-344.

[18] S. Kumar, Y. Lei, N. H. Alshareef, M. A. Quevedo-Lopez, K. N. Salama, Biofunctionalized two-dimensional Ti3C2 MXenes for ultrasensitive detection of cancer biomarker. Biosens. Bioelectron., 121 (2018) 243-249.

[19] X. Xie, M. Q. Zhao, B. Anasori, K. Maleski, C. E. Ren, J. Li, B. W. Byles, E. Pomerantseva, G. Wang, Y. Gogotsi, Porous heterostructured MXene/carbon nanotube composite paper with high volumetric capacity for sodium-based energy storage devices, Nano Energy 26 (2016) 513-523.

[20] J. Yan, C. E. Ren, K. Maleski, C. B. Hatter, B. Anasori, P. Urbankowski, A. Sarycheva, Y. Gogotsi, Flexible MXene/graphene films for ultrafast supercapacitors with outstanding volumetric capacitance, Adv. Funct. Mater. 27 (2017) 1264-1274.

[21] S. Y. Yang, K. H. Chang, Y. F. Lee, C. C. M. Ma, C. C. Hu, Constructing a hierarchical graphene-carbon nanotube architecture for enhancing exposure of graphene and electrochemical activity of Pt nanoclusters, Electrochem. Commun. 12 (2010) 1206-1209.

[22] P. Yu, G. Cao, S. Yi, X. Zhang, C. Li, X. Sun, K. Wang, Y. Ma, Binder-free 2D titanium carbide (MXene)/carbon nanotube composites for high-performance lithium-ion capacitors, Nanoscale 10 (2018) 5906-5913.

[23] Y. Wang, L. Wang, Q. Zhuang, A ratiometric electrochemical sensor for dopamine detection based on hierarchical manganese dioxide nanoflower/multiwalled carbon nanotube nanocomposite modified glassy carbon electrode. J. Alloys Compounds, 802 (2019) 326-334.

[24] M. Q. Zhao, C. E. Ren, Z. Ling, M. R. Lukatskaya, C. Zhang, K. L. Van Aken, M. W. Barsoum, Y. Gogotsi, Flexible MXene/carbon nanotube composite paper with high volumetric capacitance, Adv. Mater. 27 (2015) 339-345.

[25] Y. Cai, J. Shen, G. Ge, Y. Zhang, W. Jin, W. Huang, J. Shao, J. Yang, X. Dong, Stretchable $Ti_3C_2T_x$ MXene/carbon nanotube composite based strain sensor with ultrahigh sensitivity and tunable sensing range, ACS nano 12 (2018) 56-62.

[26] H. Momeneh, M. B. Gholivand, Mycophenolate mofetil sensor based on molecularly imprinted polymer/multi-walled carbon nanotubes modified carbon paste electrode, Anal. Biochem. 557 (2018) 97-103.

[27] D. Duan, H. Yang, Y. Ding, L. Li, G. Ma, A three-dimensional conductive molecularly imprinted electrochemical sensor based on MOF derived porous

carbon/carbon nanotubes composites and prussian blue nanocubes mediated amplification for chiral analysis of cysteine enantiomers, Electrochim. Acta 302 (2019) 137-144.

[28] Y. Teng, F. Liu, X. Kan, Voltammetric dopamine sensor based on three-dimensional electrosynthesized molecularly imprinted polymers and polypyrrole nanowires, Microchim. Acta 184 (2017) 2515-2522.

[29] W. Zhang, D. Duan, S. Liu, Y. Zhang, L. Leng, X. Li, N. Chen, Y. Zhang, Metal-organic framework-based molecularly imprinted polymer as a high sensitive and selective hybrid for the determination of dopamine in injections and human serum samples, Biosens. Bioelectron.118 (2018) 129-136.

[30] T. Qian, C. Yu, X. Zhou, P. Ma, S. Wu, L. Xu, J. Shen, Ultrasensitive dopamine sensor based on novel molecularly imprinted polypyrrole coated carbon nanotubes, Biosens. Bioelectron. 58 (2014) 237-241.

[31] F. Tan, L. Cong, X. Li, Q. Zhao, H. Zhao, X. Quan, J. Chen, An electrochemical sensor based on molecularly imprinted polypyrrole/graphene quantum dots composite for detection of bisphenol A in water samples, Sens. Actuators B 233 (2016) 599-606.

[32] W. Zheng, P. Zhang, J. Chen, W. B. Tian, Y. M. Zhang, Z. M. Sun, In situ synthesis of $CNTs@Ti_3C_2$ hybrid structures by microwave irradiation for high-performance anodes in lithium ion batteries, J. Mater. Chem. A 6 (2018) 3543-3551.

[33] X. Li, X. Yin, M. Han, C. Song, H. Xu, Z. Hou, L. Zhang, L. Cheng, Ti_3C_2 MXenes modified with in-situ grown carbon nanotubes for enhanced electromagnetic

27

wave absorption properties. J. Mater. Chem. C 5 (2017) 4068-4074

[34] J. Ai, Y. Lei, S. Yang, C. Lai, Q. Xu, SnS nanoparticles anchored on Ti_3C_2 nanosheets matrix via electrostatic attraction method as novel anode for lithium ion batteries, Chem. Eng. J. 357 (2019) 150-158.

[35] X. Yang, Q. Jia, F. Duan, B. Hu, M. Wang, L. He, Y. Song, Z. Zhang, Multiwall carbon nanotubes loaded with MoS_2 quantum dots and MXene quantum dots: Non-Pt bifunctional catalyst for the methanol oxidation and oxygen reduction reactions in alkaline solution, Appl. Surf. Sci. 464 (2019) 78-87.

[36] Q. Guan, J. Ma, W. Yang, R. Zhang, X. Zhang , X. Dong, Y. Fan, L. Cai, Y. Cao, Y. Zhang, N. Li, Q. Xu Highly fluorescent Ti_3C_2 MXene quantum dots for aacrophage labeling and Cu^{2+} ion sensing, Nanoscale 11 (2019) 14123-14133.

[37] S. S. Shankar, R. M. Shereema, R. B. Rakhi, Electrochemical determination of adrenaline using MXene/graphite composite paste electrodes, ACS Appl. Mater. Interf. 10 (2018) 43343-43351.

[38] B. Li, Y. Zhou, W. Wu, M. Liu, S. Mei, Y. Zhou, T. Jing, Highly selective and sensitive determination of dopamine by the novel molecularly imprinted poly(nicotinamide)/CuO nanoparticles modified electrode, Biosens. Bioelectron. 67 (2015) 121-128.

[39] M. Cui, J. Huang, Y. Wang, Y. Wu, X. Luo, Molecularly imprinted electrochemical sensor for propyl gallate based on PtAu bimetallic nanoparticles modified graphene-carbon nanotube composites, Biosens. Bioelectron. 68 (2015) 563-569.

[40] Z. Yang, X. Liu, Y. Wu, C. Zhang, Modification of carbon aerogel electrode with molecularly imprinted polypyrrole for electrochemical determination of dopamine, Sens. Actuators B 212 (2015) 457-463.

[41] Y. Liu, M. Wei, Y. Hu, L. Zhu, J. Du, An electrochemical sensor based on a molecularly imprinted polymer for determination of anticancer drug mitoxantrone, Sens. Actuators B 255 (2018) 544-551.

[42] F. R. Wang, G. J. Lee, N. Haridharan, J. J. Wu, Electrochemical sensor using molecular imprinting polymerization modified electrodes to detect methyl parathion in environmental media, Electrocatalysis 9 (2018) 1-9

[43] Y. Tan, J. Jin, S. Zhang, Z. Shi, J. Wang, J. Zhang, W. Pu, C. Yang, Electrochemical determination of bisphenol A using a molecularly imprinted chitosan-acetylene black composite film modified glassy carbon electrode, Electroanalysis 28 (2016) 189-96.

[44] G. Bharath, E. Alhseinat, R. Madhu, S. M. Mugo, S. Alwasel, A. H. Harrath, Facile synthesis of Au@α-Fe$_2$O$_3$@RGO ternary nanocomposites for enhanced electrochemical sensing of caffeic acid toward biomedical applications, J. Alloy. Compd 750 (2018) 819-827.

[45] X. Qiu, L. Lu, J. Leng, Y. Yu, W. Wang, M. Jiang, L. Bai, An enhanced electrochemical platform based on graphene oxide and multi-walled carbon nanotubes nanocomposite for sensitive determination of sunset yellow and tartrazine, Food.Chem. 190 (2016) 889-895.

[46] Nacano Letícia Ramos, S. M. Gava, Tarley César Ricardo Teixeira, Selective

sorbent enrichment of nickel ions from aqueous solutions using a hierarchically hybrid organic-inorganic polymer based on double imprinting concept, J. Brazil. Chem. Soc, 21(3), (2010) 419-430.

[47] D. A. Armbruster, M. D. Tillman, L. M. Hubbs, Limit of detection (LQD)/limit of quantitation (LOQ): comparison of the empirical and the statistical methods exemplified with GC-MS assays of abused drugs. Clinical chemistry, 40(7) (1994) 1233-1238.

[48] S. Xu, Y. Shao, K. Ma, Q. Cui, G. Liu, F. Wu, DNA abasic site-based aptamer for selective fluorescence light-up detection of fisetin by excited-state intramolecular proton transfer. Sens. Actuators B 171 (2012) 666-671.

[49] F. Fang, J. M. Li, Q. H. Pan, W. D. Huang, Determination of red wine flavonoids by HPLC and effect of aging. Food Chem. 101(1)(2007) 428-433

Biographies

Xue Ma is a graduate student at College of Science of Jiangxi Agricultural University. Her current research is mainly focused on electrochemical sensors.

Xiaolong Tu is a graduate student at College of Science of Jiangxi Agricultural University. His current research is mainly focused on electrochemical sensors.

Feng Gao is a graduate at College of Science of Jiangxi Agricultural University. Her research interests cover on electrochemical sensors.

Yu Xie is a graduate student at College of Science of Jiangxi Agricultural University.

Her current research is mainly focused on electrochemical sensors.

Xigen Huang **is a teacher** at Jiangxi Agricultural University. His research interests cover on electrochemical sensors.

Carlos Fernandez **is a Lecturer at Robert Gordon University in the UK. His research interests focuses on the use of voltammetric techniques in analytical chemistry as an electrochemical sensor to detect the analytes of heavy metals drugs of abuse, amino acids, pharmaceutical drugs.**

Fengli Qu is a professor at Qufu normal University in Shandong Province (China) in 2008. She worked in CPME-CNRS (Nancy, France) as a postdoctoral fellow from 2008 to 2009 and as a Visiting Professor in Princeton University (Princeton, USA) from 2013 to 2014. Currently, she is a Professor in the College of Chemistry and Chemical Engineering at Qufu Normal University. Her research interests include nanomaterial applications and biosensor development.

Guangbin Liu is an associate researcher at Jiangxi Agricultural University. His research interests cover on electrochemical sensors.

Limin Lu obtained his Ph.D. degree from the in analytical chemistry from Hunan University in 2011. He is currently an associate professor of Jiangxi Agricultural University, China. His research interests focus on electrochemical (bio) sensors.

Yongfang Yu **is a teacher** at Jiangxi Agricultural University. Her research interests cover on electrochemical sensors.

Figure captions
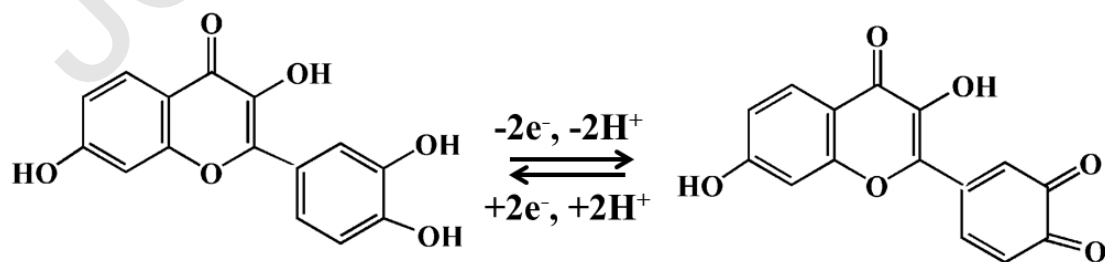
Scheme 1 Schematic illustration for the preparation of MIP/MXene/NH$_2$-CNTs/GCE

and the adsorption mechanism in the imprinted cavity.
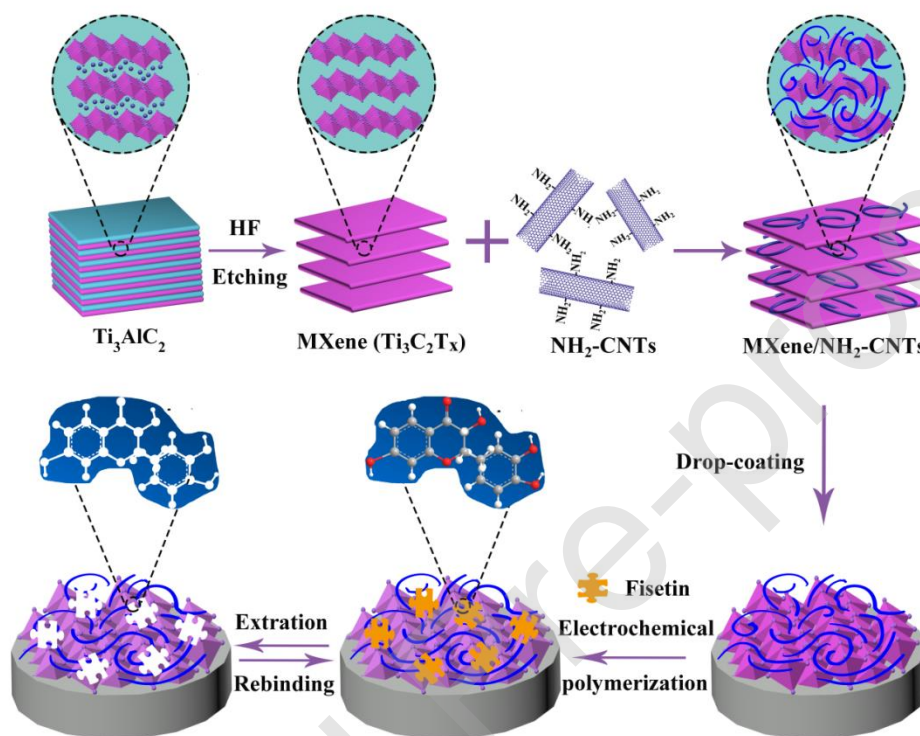
Scheme 1

Scheme 2 The reaction mechanism for the electrochemical oxidation of fisetin.

Scheme 2

Fig. 1 SEM of (A) MXene, (B) MXene/NH$_2$-CNTs composite, (C) MIP-MXene/NH$_2$-CNTs/GCE before and after (D) treatment with eluent, (E) NIP-MXene/NH$_2$-CNTs/GCE and (F) MIP/GCE.
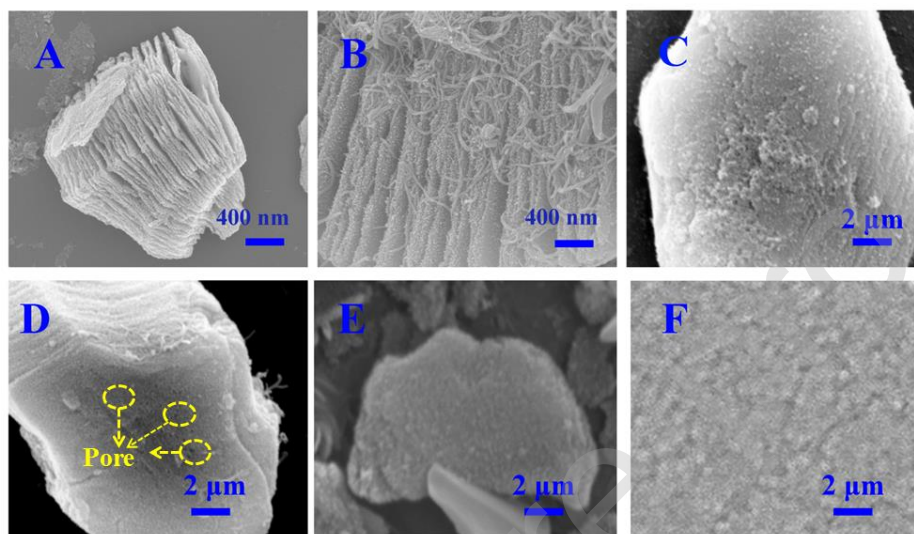

Fig. 1

Fig. 2 Survey spectra (A) of MXene (a) and MXene/NH$_2$-CNTs (b); (B) C1s XPS spectra of MXene/NH$_2$-CNTs, (C) Ti 2p XPS spectra of MXene/NH$_2$-CNTs and (D) O1s XPS spectra of MXene/NH$_2$-CNTs.
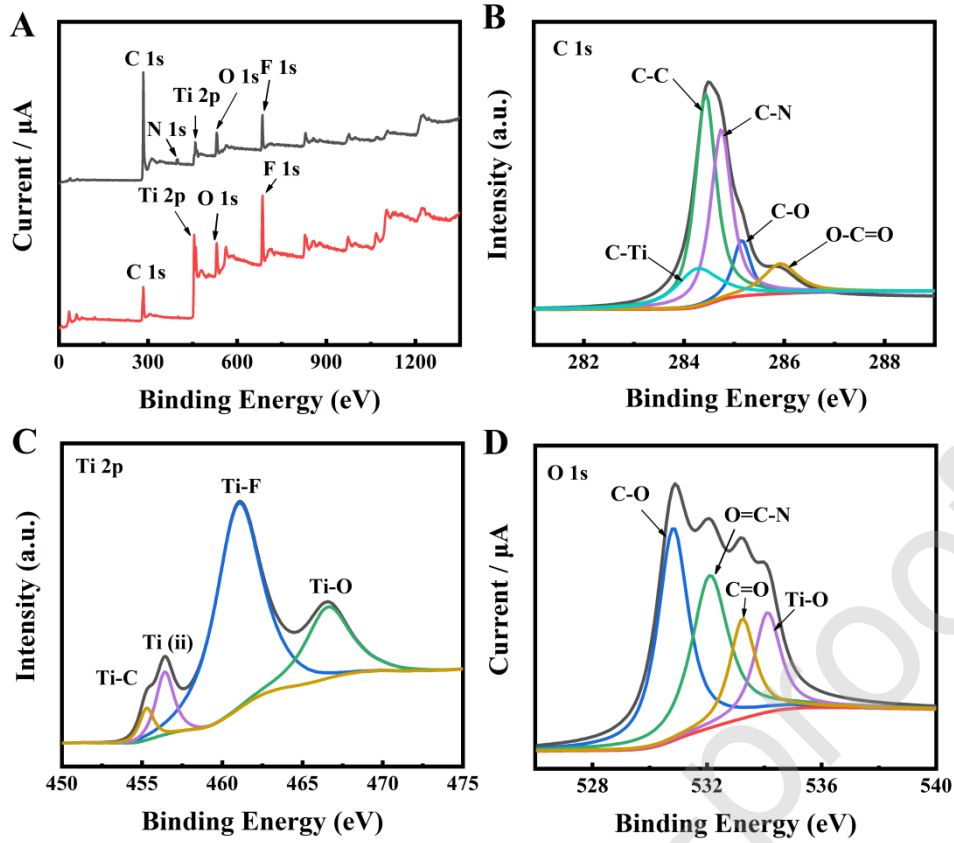
Fig. 2

Fig. 3 The XRD patterns of the pure MXene (a) and MXene/NH$_2$-CNTs (b).
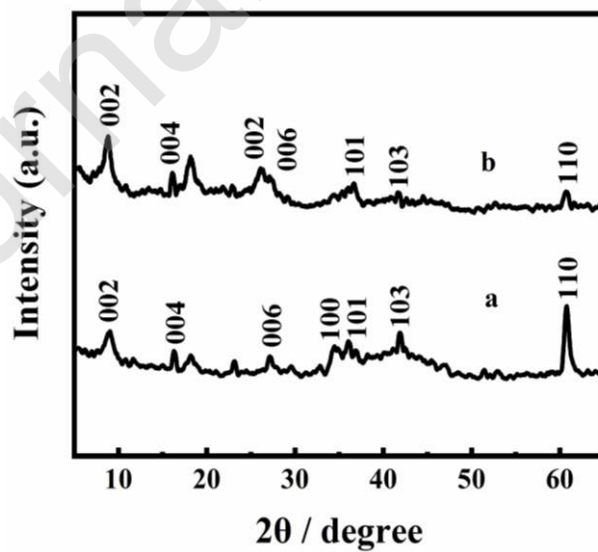
Fig. 3

Fig. 4 (A) EIS of different electrodes: (a) bare GCE, (b) MXene/GCE, (c) NH₂-CNTs/GCE and (d) MXene/NH₂-CNTs/GCE in 5 mmol L⁻¹ [Fe(CN)₆]³⁻/⁴⁻ solution containing 0.1 mol L⁻¹ KCl; (B) Cyclic voltammograms at bare GCE (a), MXene/NH₂-CNTs/GCE (b), MIP/MXene/NH₂-CNTs/GCE (c) before template removal, MIP/MXene/NH₂-CNTs/GCE (d) after template removal and (e) MIP/MXene/NH₂-CNTs/GCE after rebinding at the range of -0.2 V - 0.6 V at 100 mV s⁻¹ in 5 mmol L⁻¹ [Fe(CN)₆]³⁻/⁴⁻ solution containing 0.1 mol L⁻¹ KCl; (C) CVs of different electrodes: (a) bare GCE, (b) MIP/GCE, (c) NIP/MXene/NH₂-CNTs/GCE and (d) MIP/MXene/NH₂-CNTs/GCE in 0.1 mol L⁻¹ PBS (pH 7.0) after incubation in 20.0 µmol L⁻¹ fisetin for 150 s.
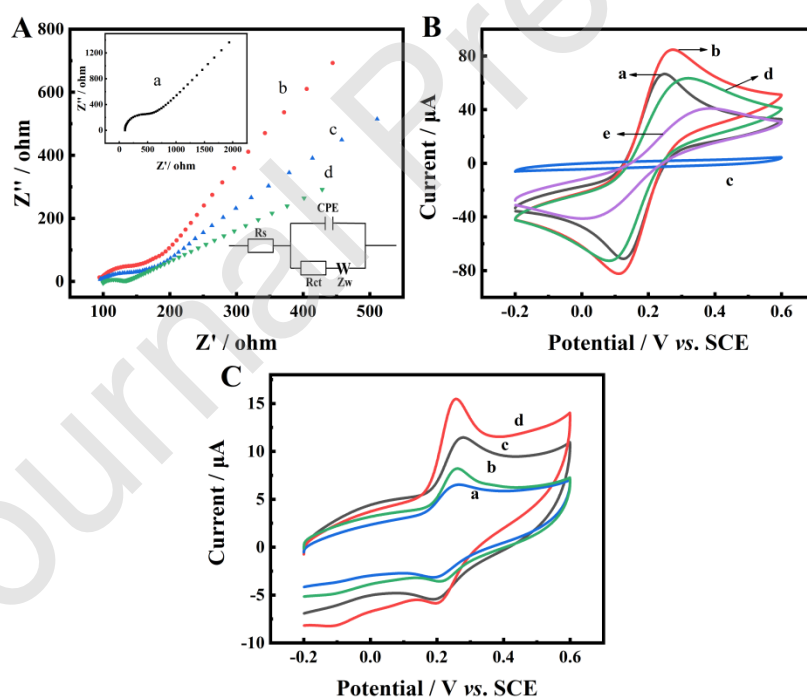

Fig. 4

Fig. 5 (A) Effect of electropolymerization cycles on current response; (B) Effect of

the ratio of template molecules to functional monomers on current response; (C) Effect of extraction time on current response; (D) Effect of pH of supporting electrolyte on current response; (E) Effect of incubation time on current response.
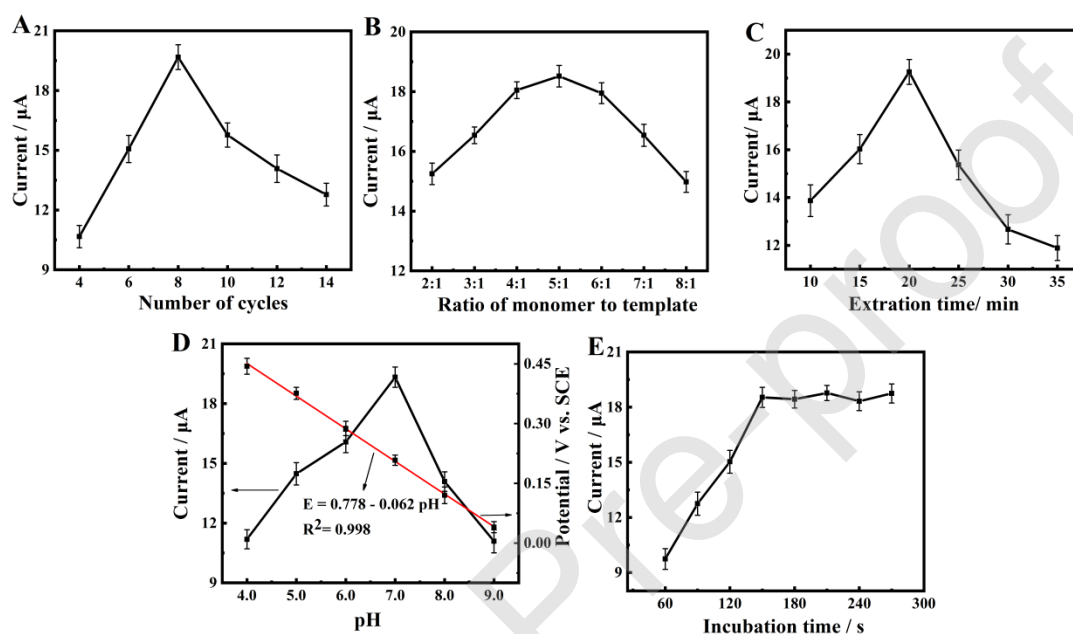

Fig. 5

Fig. 6 (A) CVs of 20.0 μmol L^{-1} fisetin on MIP/MXene/NH$_2$-CNTs/GCE in 0.1 mol L^{-1} PBS (pH 2.0) at different scan rates: 20, 40, 60, 80, 100, 120, 140, 160, 180, 200, 220, 240, 260, 280 and 300 mV s^{-1}; (B) Linear relationship between the redox peak current value and the scan rates; (C) Linear relationship between redox peak potential (E_p) and the natural logarithm of scan rate (ln v).
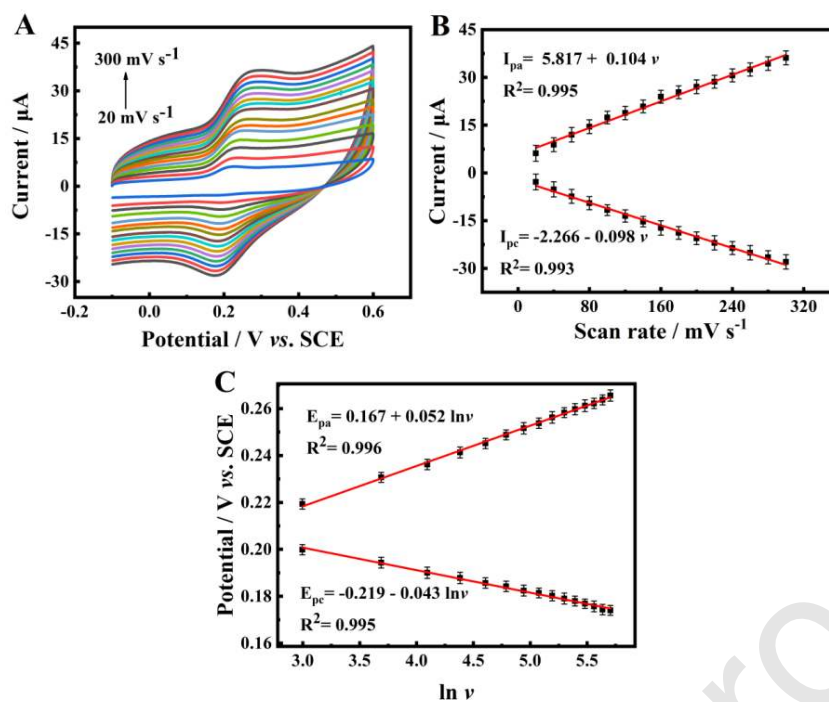
37

Fig. 6

Fig. 7 DPV of different fisetin concentrations (0.003, 0.007, 0.01, 0.05, 0.3, 0.7, 1, 3, 5, 7, 10, 15 and 20.0 μmol L^{-1}) at the MIP/MXene/NH$_2$-CNTs/GCE. Insert: the corresponding calibration plot for the MIP/MXene/NH$_2$-CNTs/GCE and DPV for fisetin concentration from 0.003 to 1.0 μmol L^{-1}.
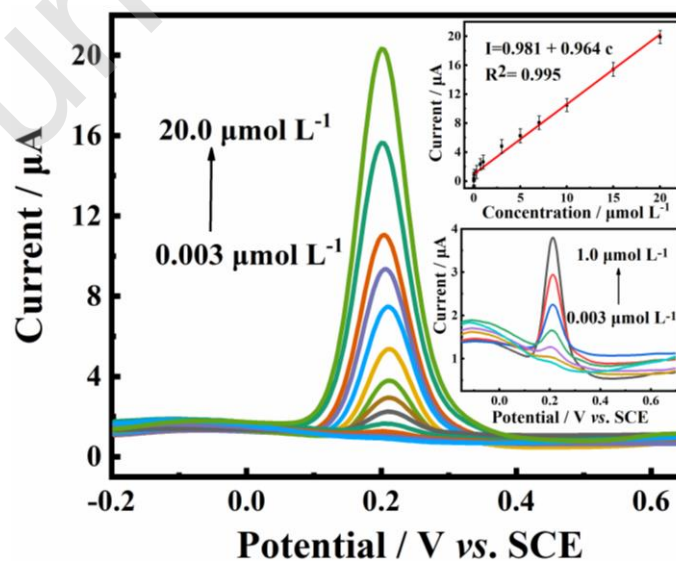
Fig. 7

Fig. 8 (A) DPV responses of MIP/MXene/NH₂-CNTs/GCE in 0.1 µmol L⁻¹ PBS (pH= 7.0) containing 20.0 µmol L⁻¹ fisetin and 50-folds interferences; (B) DPV response of MIP/MXene/NH₂-CNTs/GCE for six different electrodes; (C) The stability of MIP/MXene/NH₂-CNTs/GCE.
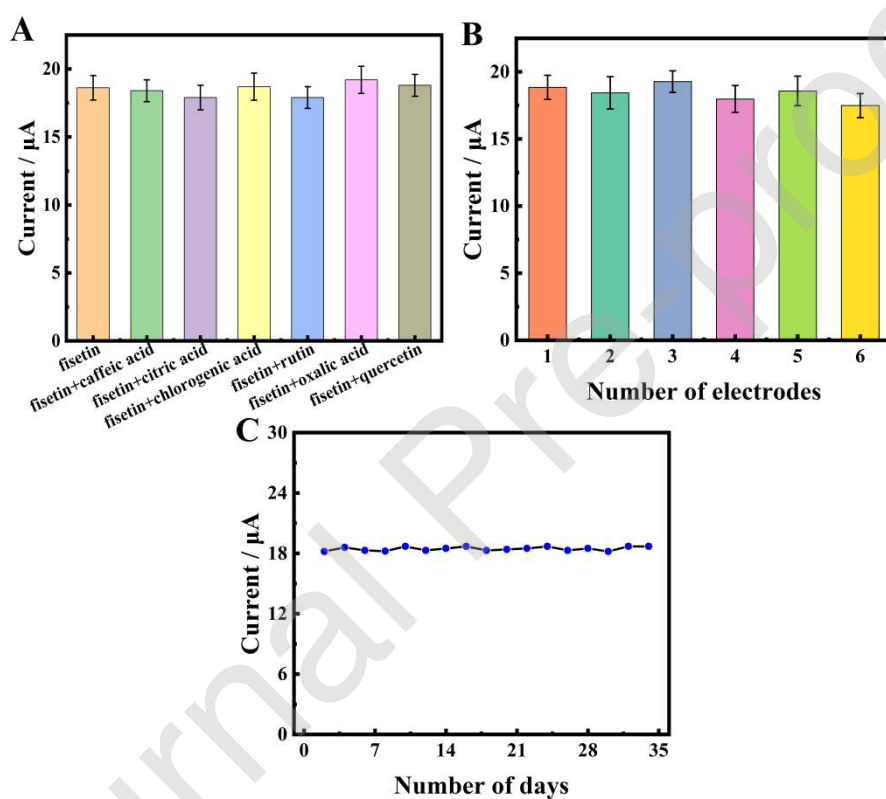

Fig. 8

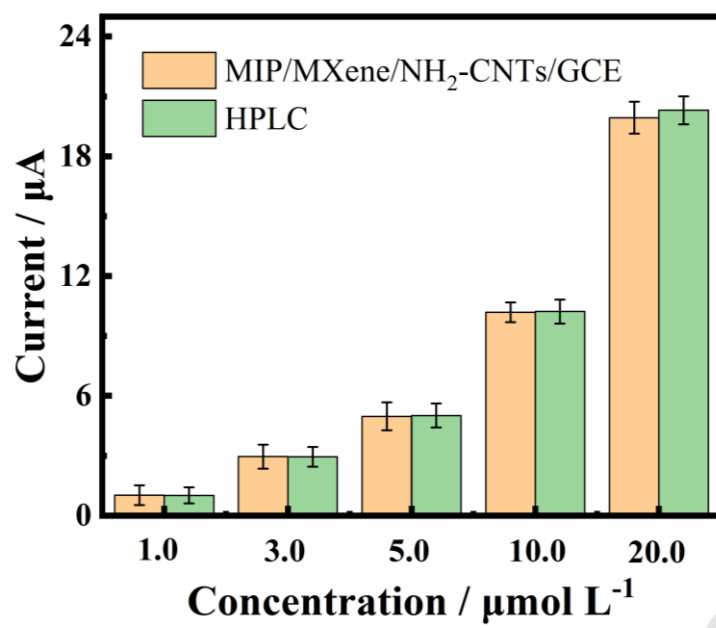**Fig. 9** Performance comparison of MIP/MXene/NH₂-CNTs/GCE and HPLC.

Fig. 9

Table 1 Comparison of the electrochemical sensing performance of different method toward fisetin detection.

Detection method	Linear range (μmol L^{-1})	Detection limit (nmol L^{-1})	Reference
Au-BMI.PF6[a]	0.28 - 19.5	50	[3]
SAM[b]	0.1 - 100	500	[8]
Fluorescence light-up	0.1 - 5	50	[48]
HPLC[c]	5.47 - 87.55	52	[49]
MIP-MXene/NH$_2$-CNTs/GCE	0.003 - 20.0	1	This work

a: gold nanoparticles in ionic liquid and binuclear nickel complex immobilized in silica;

b: self-assembled monolayers;

c: high performance liquid chromatography.

Table 2 Detection of fisetin in real samples (n= 4).

cotinus coggygria leaves	Added (μmol L^{-1})	Found (μmol L^{-1})	RSD (%)	Recovery (%)
1	1.00	1.03	2.28	103.0
2	3.00	2.96	4.32	98.7
3	5.00	4.98	3.45	99.6
4	10.00	10.19	3.62	101.9
5	20.00	19.94	4.09	99.7